International Journal of Engineering Science 62 (2013) 70–83

Contents lists available at SciVerse ScienceDirect

International Journal of Engineering Science

journal homepage: www.elsevier.com/locate/ijengsci

Magnetoelectricity in coated fibrous composites of piezoelectric and piezomagnetic phases

Hsin-Yi Kuo *, Cheng-You Peng

Department of Civil Engineering, National Chiao Tung University, Hsinchu 30010, Taiwan

ARTICLE INFO

Article history:
Received 3 May 2012
Received in revised form 19 July 2012
Accepted 12 August 2012
Available online 5 October 2012

Keywords:
Magnetoelectricity
Coated fibrous composites
Piezoelectric
Piezomagnetic
Micromechanics
Finite element analysis

ABSTRACT

This paper studies the effective magnetoelectric (ME) behavior of coated fibrous composites made of piezoelectric and piezomagnetic phases. We employ a micromechancial model, the two-level recursive scheme together with the Mori–Tanaka method, to evaluate the ME effect of the composites. The magnitudes and trends of the solutions are in good agreement with the calculations by the finite element analysis. Based on this model, we find the optimal volume fractions of the inclusion, the ratio of the radii between the core and shell for maximum ME coupling. Further, we correlate the ME effect with the material parameters of the constituent phases and propose useful engineering guide to the development of new ME coated fibrous composites.

1. Introduction

Magnetoelectric (ME) materials, which coexist magnetic and electric orderings, have stimulated considerable scientific and technological interest in recent years for potential applications, such as ME data storage and switching, magnetic field detectors, and electric control of magnetism (Eerenstein, Mathur, & Scott, 2006; Fiebig, 2005; Spaldin & Fiebig, 2005). However, the ME effect in natural materials is rather weak and is often observed at low temperature (Astrov, 1960; Rado & Folen, 1961). Therefore, various researchers have turned to composites made of piezoelectric (PE) and piezomagnetic (PM) media to enhance the magnetoelectricity, as explained in recent reviews by Nan, Bichurin, Dong, Viehland, and Srinivasan (2008) and Srinivasan (2010). This much stronger ME effect could be realized using product property (Nan, 1994):

$$\text{ME effect} = \frac{\text{electric}}{\text{mechanical}} \times \frac{\text{mechanical}}{\text{magnetic}}.$$

It means that an applied magnetic field causes an elastic strain in the piezomagnetic material, and this strain is translated into the electric polarization, hence electric fields, in the piezoelectric material, or vice versa.

The promise of applications have also made ME composites the topic of a number of theoretical studies (Nan et al., 2008; Zheng et al., 2004). For example, the classical Eshelby's equivalent inclusion approach and the Mori–Tanaka mean-field model have been generalized to multiferroic composites by Li and Dunn (1998a, 1998b), Wu and Huang (2000), Huang and Zhou (2004), Srinivas et al. (2006) and Liu and Kuo (2012). The analysis for local fields is available for simple microstructures such

* Corresponding author.
E-mail address: hykuo@mail.nctu.edu.tw (H.-Y. Kuo).

0020-7225/$ - see front matter © 2012 Elsevier Ltd. All rights reserved.
http://dx.doi.org/10.1016/j.ijengsci.2012.08.002

as a single inclusion (Huang & Kuo, 1997), laminates (Bichurin et al., 2003; Kuo et al., 2010; Liverts et al., 2010; Srinivas et al., 2001), and periodic array of circular/elliptic fibrous ME composites (Dinzart and Sabar, 2011; Kuo, 2011; Kuo and Pan, 2011). Homogenization methods were also proposed for periodic ME fibrous composites (Aboudi, 2001; Camacho-Montes et al., 2009), while numerical methods based on the finite element analysis have been developed to address ME composites with more general microstructures (Lee et al., 2005; Liu et al., 2004).

Recently, some three-phase multiferroic composites were made experimentally to enhance the ME coupling. Among them, Nan et al. (2002) and Nan et al., 2003 made a Terfenol-D/PZT/PVDF mixture and enhanced the ME coefficient to 45 mV/cm. Dong et al. (2006) prepared a $MnZnFe_2O_4$/Terfenol-D/PZT laminate, and found the enhanced ME field coefficients of up to 8–28 times of those of Terfenol-D/PZT counterpart. Gupta and Chatterjee (2009) prepared a three-phase $BaTiO_3/CoFe_2O_4$/PVDF particulate composite, and showed a maximum ME voltage around 26 mV/cmOe. Jadhav et al. (2009) prepared a $Ni_{0.5}Cu_{0.2}Zn_{0.3}Fe_2O_4/BaTiO_3$/PZT combination and measured a maximum ME coefficient of 975 μV/cmOe. For theoretical investigations on this part, Kuo (2011) and Kuo and Pan (2011) estimate the overall behavior of multiferroic composites with coated circular/elliptic fibrous under generalized anti-plane deformation. Dinzart and Sabar (2011) employed Green's functions techniques, interfacial operators, and Mori–Tanaka's model for solving the magneto-electro-elastic coated inclusion problem. Later, Kuo and Wu (2012) proposed a micromechanical model, the two-level recursive scheme in conjunction with the Mori–Tanaka method, to a core–shell-matrix particulate multiferroic composite. They showed that the solutions are in good agreement with the prediction by the finite element analysis. In the present study, we follow this similar idea to investigate the effective property of a coated fibrous composites made of piezoelectric and piezomagnetic phases.

The plan of this article is organized as follows: in Section 2, we formulate the basic equations for a piezoelectric-piezomagnetic composite and define the effective properties of the heterogeneous media. In Section 3 we present a micromechanical approach to estimate the overall behavior of core–shell-matrix, three-phase multiferroic fibrous composites. We introduce the finite element analysis in Section 4. Both methodologies are illustrated in Section 5. We study how the ME voltage coefficient depends on the radius ratio of the core and shell, volume fractions of the fiber phase, and material properties of constituent phases. Furthermore, we improve the ME coupling by tuning the material parameters, and summarize a few useful design principles.

2. Problem statement

2.1. Basic equations

Let us consider a coated fibrous composite made of piezoelectric and piezomagnetic materials as shown in Fig. 1. The cylinders are infinitely long with fibers aligned in x_3-direction. The composite is consisting of a continuous matrix phase, m, in which there are embedded inhomogeneities of a circular core phase, c, and a shell phase, s, which represents a layer of coating that encloses the core phase. The radii of the core and coating are a and b, respectively, and the ratio between them is defined as $\gamma \equiv a/b$. The general constitutive laws for the rth phase are given by (see Alshits et al., 1992, for example)

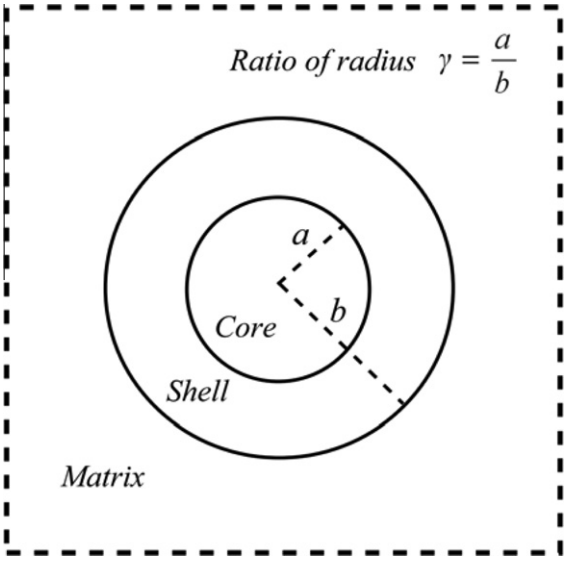

Fig. 1. The cross-section of a circular coated fibrous composite.

$$\begin{aligned}\sigma_{ij}^{(r)} &= C_{ijkl}^{(r)}\varepsilon_{kl}^{(r)} - e_{lij}^{(r)}E_l^{(r)} - q_{lij}^{(r)}H_l^{(r)},\\ D_i^{(r)} &= e_{ikl}^{(r)}\varepsilon_{kl}^{(r)} + \kappa_{il}^{(r)}E_l^{(r)} + \lambda_{li}^{(r)}H_l^{(r)},\\ B_i^{(r)} &= q_{ikl}^{(r)}\varepsilon_{kl}^{(r)} + \lambda_{il}^{(r)}E_l^{(r)} + \mu_{il}^{(r)}H_l^{(r)},\end{aligned} \tag{2.1}$$

where σ_{ij}, D_i, B_i, ε_{ij}, E_i and H_i are the stress, electric displacement, magnetic flux, strain, electric field and the magnetic field, respectively. C_{ijkl} is the elastic moduli; e_{ikl} and q_{ikl} are the piezoelectric and piezomagnetic constants; κ_{il}, μ_{il} and λ_{il} are the dielectric permittivity, magnetic permeability and magnetoelectric coefficient. The symmetry conditions satisfied by the moduli are given by Nye (1985).

The strain, ε_{ij}, electric field, E_i, and magnetic field, H_i are respectively defined by the displacement u_i, electric potential φ, and magnetic potential ψ via

$$\varepsilon_{ij} = \frac{1}{2}(u_{i,j} + u_{j,i}), \quad E_i = -\varphi_{,i}, \quad H_i = -\psi_{,i}. \tag{2.2}$$

On the other hand, the balance of linear momentum, Gauss's law, and the condition of no magnetic poles give that the stress, electric displacement, and magnetic flux satisfy the following equilibrium equations

$$\sigma_{ij,j} = 0, \quad D_{i,i} = 0, \quad B_{i,i} = 0. \tag{2.3}$$

These differential equations can be solved, subject to suitable interface and boundary conditions. We assume that the interfaces are perfectly bonded, and therefore the field quantities satisfy

$$\begin{aligned}&[\![\sigma_{ij}n_j]\!] = 0, \quad [\![D_i n_i]\!] = 0, \quad [\![B_i n_i]\!] = 0,\\ &[\![u_i]\!] = 0, \quad [\![\varphi]\!] = 0, \quad [\![\psi]\!] = 0,\end{aligned} \tag{2.4}$$

where $[\![\cdot]\!]$ denotes the jump in some quantity across the interface, and n_i is the unit outward normal to the interface.

For convenience, we rewrite the constitutive laws (2.1) in the matrix notation as (Alshits et al., 1992)

$$\boldsymbol{\Sigma} = \mathbf{L}\mathbf{Z}, \tag{2.5}$$

with

$$\boldsymbol{\Sigma} = \begin{bmatrix}\boldsymbol{\sigma}\\ \mathbf{D}\\ \mathbf{B}\end{bmatrix}, \quad \mathbf{Z} = \begin{bmatrix}\boldsymbol{\varepsilon}\\ -\mathbf{E}\\ -\mathbf{H}\end{bmatrix}, \quad \mathbf{L} = \begin{bmatrix}\mathbf{C} & \mathbf{e}^t & \mathbf{q}^t\\ \mathbf{e} & -\boldsymbol{\kappa} & -\boldsymbol{\lambda}^t\\ \mathbf{q} & -\boldsymbol{\lambda} & -\boldsymbol{\mu}\end{bmatrix}. \tag{2.6}$$

Here the superscript t denotes the transpose of the matrix.

2.2. Effective moduli

In this study, we are interested in determining the overall properties of multiferroic composites. The macroscopic properties are defined in terms of average fields,

$$\langle\boldsymbol{\Sigma}\rangle = \mathbf{L}^*\langle\mathbf{Z}\rangle, \tag{2.7}$$

where $\mathbf{L}^*$ denotes the macroscopic magnetoelectroelastic coefficients of the heterogeneous material, and the angular brackets denote the average over the representative volume element (RVE). Note that, although in each component, the magnetoelectric coefficient is zero, i.e., $\boldsymbol{\lambda} = \mathbf{0}$, the coupling effect $\boldsymbol{\lambda}^*$ may be non-zero.

Due to the linearity, the generalized strain in the rth phase for a matrix-based multiphase multiferroic composite is given by (Srinivas et al., 2006)

$$\mathbf{Z}_r = \mathbf{A}_r\langle\mathbf{Z}\rangle, \tag{2.8}$$

where $\mathbf{A}_r$ is the generalized strain concentration tensor of the rth phase, satisfying $\sum_{r=1}^{N}\mathbf{A}_r = \mathbf{I}$, where $\mathbf{I}$ is the fourth-order identity tensor. As a result, from the average generalized stress and strain theorems, the effective moduli can be determined for a $(N+1)$-phase composite as

$$\mathbf{L}^* = \mathbf{L}_m + \sum_{r=1}^{N} f_r(\mathbf{L}_r - \mathbf{L}_m)\mathbf{A}_r. \tag{2.9}$$

Here f_r is the volume fraction of the rth phase. The concentration tensor can be determined by various micromechanical models, which will be discussed in the following section.

3. Micromechanical approach

To estimate the effective moduli, $\mathbf{L}^*$, of multiferroic composites, we first turn to the direct Mori–Tanaka method, which approximates the coated particle problem using a composite with distinct particles representing the core and shell phases

(Fisher and Brinson, 2001). This gives the effective properties of the core–shell-matrix mutliferroic as Eq. (2.9), with the concentration tensor for the core ($j = 1$) and shell ($j = 2$)

$$\mathbf{A}_j = \mathbf{A}_j^{dil}\left(f_m\mathbf{I} + f_c\mathbf{A}_1^{dil} + f_s\mathbf{A}_2^{dil}\right)^{-1}, \quad j = 1, 2. \tag{3.1}$$

Here

$$\mathbf{A}_j^{dil} = \left[\mathbf{I} + \mathbf{S}_j\mathbf{L}_m^{-1}(\mathbf{L}_j - \mathbf{L}_m)\right]^{-1}, \tag{3.2}$$

$\mathbf{S}_j$ is the magnetoelectroelastic Eshelby tensor, which is a function of the magnetoelectroelastic moduli of matrix, the shape and orientation of the jth inclusion, and is described by (Li and Dunn, 1998b)

$$S_{MnAb} = \frac{1}{8\pi}L_{ijAb}\begin{cases} \int_{-1}^{1}\int_{0}^{2\pi}[G_{mJin}(z_j) + G_{nJim}(z_j)]d\theta d\xi_3, & M = 1, 2, 3, \\ 2\int_{-1}^{1}\int_{0}^{2\pi}G_{4Jin}(z_j)d\theta d\xi_3, & M = 4, \\ 2\int_{-1}^{1}\int_{0}^{2\pi}G_{5Jin}(z_j)d\theta d\xi_3, & M = 5. \end{cases} \tag{3.3}$$

In the above equation, $z_i = \xi_i/a_i$ (no summation on i), a_i is the semi-axis of size, and ξ_1 and ξ_2 can be expressed in terms of ξ_3 and θ by $\xi_1 = \sqrt{1-\xi_3^2}\cos\theta$ and $\xi_2 = \sqrt{1-\xi_3^2}\sin\theta$. In addition $G_{MJin} = z_i z_n K_{MJ}^{-1}(z_j)$, where K_{MJ}^{-1} is the inverse of $K_{JR} = z_i z_n L_{ijRn}$. Li and Dunn (1998a) have obtained the closed-form expressions of magnetoelectroelastic Eshelby's tensors for the aligned elliptic cylinder inclusion in a transversely isotropic medium. For the coated fibrous composites with arbitrary crystal symmetry as we discussed in this work, we resort to Gauss quadrature numerical method to calculate S_{MnAb}. The integral (3.3) then is approximated by the weighted sum of function values at certain integration points (Li, 2000).

However, we will show later that this prediction deviates largely from that determined by the finite element analysis. Therefore, the direct Mori–Tanaka method is not good in estimating the coupling constants. We now turn to another approach, the two-level recursive scheme with the Mori–Tanaka technique. The basic concept of the two-level recursive scheme is that the matrix sees coated particles that are themselves composites. This procedure was first used to predict the behavior of viscoelastic composites containing multiphases of coated inclusions (Friebel et al., 2006). At the deepest level, each coated particulate inclusion is seen as a two-phase composite, which, once homogenized, plays the role of a homogeneous inclusion for the matrix material (highest level).

Further, at each level, we employ the Mori–Tanaka approach in prediction the effective moduli of the corresponding two-phase composite. Based on this model, at the deepest level, the coated inclusions are seen as a two-phase composite with effective moduli

$$\mathbf{L}_{sc}^{*} = \mathbf{L}_s + \frac{f_c}{f_i}(\mathbf{L}_c - \mathbf{L}_s)\mathbf{A}_c. \tag{3.4}$$

Here, the subscripts c, s, and i represent core, shell and inclusion (core plus shell), respectively. The concentration tensor $\mathbf{A}_c$ can be determined as

$$\mathbf{A}_c = f_i\mathbf{A}_c^{dil}\left(f_s\mathbf{I} + f_c\mathbf{A}_c^{dil}\right)^{-1}, \tag{3.5}$$

with the dilute concentration tensor $\mathbf{A}_c^{dil}$ given by

$$\mathbf{A}_c^{dil} = \left[\mathbf{I} + \mathbf{S}_c\mathbf{L}_s^{-1}(\mathbf{L}_c - \mathbf{L}_s)\right]^{-1}. \tag{3.6}$$

Here $\mathbf{S}_c$ is the generalized Eshelby tensor for the core phase, which is a function of the property of the shell, and the shape and orientation of the core phase.

At the highest level, the effective coated fibers play the role of reinforcements and, similarly, we have the effective behavior

$$\mathbf{L}^{*} = \mathbf{L}_m + f_i(\mathbf{L}_{sc} - \mathbf{L}_m)\mathbf{A}_{sc}. \tag{3.7}$$

Again the concentration tensor can be determined as

$$\mathbf{A}_{sc} = \mathbf{A}_{sc}^{dil}\left(f_m\mathbf{I} + f_c\mathbf{A}_{sc}^{dil}\right)^{-1}, \tag{3.8}$$

with the dilute concentration tensor

$$\mathbf{A}_{sc}^{dil} = \left[\mathbf{I} + \mathbf{S}_{sc}\mathbf{L}_m^{-1}(\mathbf{L}_{sc}^{*} - \mathbf{L}_m)\right]^{-1}. \tag{3.9}$$

Here $\mathbf{S}_{sc}$ is the generalized Eshelby tensor for effective coated fibers, which is a function of the moduli of the matrix, and the shape and orientation of the coated fibers (core plus shell).

4. Finite element method

In this section, we introduce the finite element method which is used for comparison with the above micromechanical solutions. We first choose an appropriate representative volume element (RVE), a periodic unit cell, which captures the major features of the underlying microstructure. There are five possible ways of packing cylinders in regular arrays in two dimensions (see Kittel, 2005, for instance). Here we concentrate on the two lattices, square and hexagonal arrangements (Fig. 2).

Further, due to the periodicity in the composite structure, the displacement, u_i, electric potential, φ, and the magnetic potential, ψ, in any point of the unit cell can be expressed in terms of those at an equivalent point in another RVE such that the periodic boundary conditions

$$\begin{aligned}
&\Phi(d,x_2,x_3) = \Phi(-d,x_2,x_3) + \langle \Phi_{,1} \rangle 2d,\\
&\Phi(x_1,d,x_3) = \Phi(x_1,-d,x_3) + \langle \Phi_{,2} \rangle 2d,\\
&\Phi(x_1,x_2,d) = \Phi(x_1,x_2,-d) + \langle \Phi_{,3} \rangle 2d
\end{aligned} \tag{4.1}$$

are satisfied for a square lattice. Here Φ is the component of u_i, φ, or ψ, and $2d$ is the length of the unit cell. The comma in the subscript denotes the partial derivative. Similarly, the periodic boundary conditions for a hexagonal lattice are

$$\begin{aligned}
&\Phi(d,x_2,x_3) = \Phi(-d,x_2,x_3) + \langle \Phi_{,1} \rangle 2d,\\
&\Phi\left(x_1,\sqrt{3}d,x_3\right) = \Phi\left(x_1,-\sqrt{3}d,x_3\right) + \langle \Phi_{,2} \rangle 2\sqrt{3}d,\\
&\Phi(x_1,x_2,d) = \Phi(x_1,x_2,-d) + \langle \Phi_{,3} \rangle 2d.
\end{aligned} \tag{4.2}$$

In order to evaluate the effective coefficients of the above periodic multiferroic composite, the strain, ε_{ij}, electric field, E_i, and magnetic field states, H_i are applied individually to the unit cell. The periodic boundary conditions have to be applied to the unit cell in such a way that, apart from one component of the strain, electric field, or magnetic field $\langle \Phi_{,i} \rangle$ in Eqs. (4.1) or (4.2), all other components are made equal to zero. Then each effective constant can be determined by (2.7). We perform the three-dimensional finite element analysis using the software COMSOL Multiphysics.

5. Results and discussion

As a numerical example, we take a composite made of PE cores coated PM shell in a PM matrix. For the piezoelectric material, we first choose the widely used $BaTiO_3$ (BTO) ceramic as the core phase. For the piezomagnetic material we choose $CoFe_2O_4$ (CFO) as the shell phase while Terfenol-D (TD) as the matrix phase. They are all transversely isotropic, i.e. with 6 mm

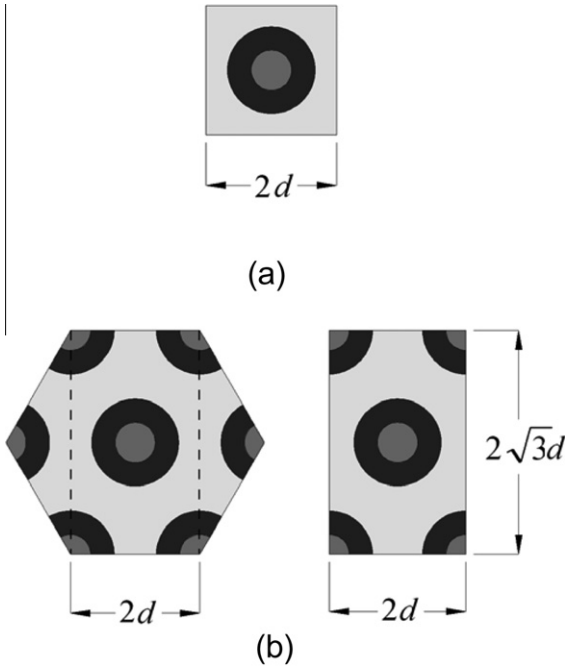

Fig. 2. A schematic representation of a unit cell. (a) A square array. (b) A hexagonal array.

symmetry. For convenience, we denote the composite as BTO/CFO/TD. The independent material constants of these constituents are given in Table 1 in Voigt notation, where the x_1x_2 plane is isotropic and the poling direction/magnetic axis is along the x_3-direction.

In this study, a material property of particular interest is the ME voltage coefficient $\alpha^*_{E,ij} = \lambda^*_{ij}/\kappa^*_{ij}$ (no summation), where $\lambda^*_{ij}\left(\kappa^*_{ij}\right)$ is the effective ME coupling coefficient (dielectric permittivity) of the composite. The effective ME voltage coefficient $\alpha^*_{E,ij}$, which relates the overall electric field generated in the composite with the applied magnetic field, is the figure of merit for magnetic field sensors.

Fig. 3 shows how the ME voltage coefficient depends on the inclusion volume fraction, f_i, and the ratio of radii, γ, for the BTO/CFO/TD three-phase multiferroic composite. The ME voltage coefficient is non-zero for every non-zero volume fraction of the inclusion even though this coefficient is zero for each constituent phase. This reflects the ME coupling is mediated by the elastic interaction. In the micromechanical approach, there is no upper limit on the volume fractions, since Mori–Tanaka's model is a mean-field theory. On the other hand, the finite element analysis is estimated for discrete volume fractions and stops around $f_i = \pi/4$ and $f_i = \pi/2\sqrt{3}$ for the square and hexagonal arrays, respectively, when the inclusions begin to touch each other. The prediction of the two-level recursive scheme together with the Mori–Tanaka's approach is in good agreement with the results of the finite element analysis. The maximum ME voltage coefficient $\alpha^*_{E,11}$ is -7.8359 V/cmOe at volume fraction $f_i = 0.86$ with $\gamma = 0.7$ (Fig. 3(a)). On the other hand, the maximum $\alpha^*_{E,33}$ is 1.3425 V/cmOe at volume fraction $f_i = 1$ with $\gamma = 0.3$, which corresponds to the two-phase composite BTO/CFO (Fig. 3(b)). Note that the results of the hexagonal array are closer to the Mori–Tanaka's estimation than those of the square array. This is because a hexagonal array is a closed packing structure, and the Mori–Tanaka model allows the inclusion to fulfill the matrix.

Fig. 3(a) and (b) also compare with the effective ME voltage coefficients predicted by Kuo and Pan (2011) who used multipole expansion technique. Still, the overall magnitudes and trends agree well among predictions based on the micromechanical model, finite element analysis, and Kuo and Pan's model. Further, Fig. 3 compares the overall moduli with those calculated by the direct Mori–Tanaka method for the case $\gamma = 0.8$. It is observed that the prediction deviates largely from those determined by the finite element analysis. Therefore, the direct Mori–Tanaka method is not good in estimating the coupling constants, although calculations show that they evaluate elastic stiffness well.

Finally, for comparison, Fig. 3 also shows the effective moduli of the composite made by the corresponding two-phase medium (BTO/TD). It shows that the ME voltage coefficients in the coated fibrous composite can be indeed increased compared to this two-phase counterpart.

Next, we study how the effective ME voltage coefficient depends on the elastic moduli, $\mathbf{C}_{PE}$ and $\mathbf{C}_{PM}$, dielectric permittivity, $\boldsymbol{\kappa}_{PE}$ and $\boldsymbol{\kappa}_{PM}$, and magnetic permeability, $\boldsymbol{\mu}_{PE}$ and $\boldsymbol{\mu}_{PM}$, of the PE and PM materials, piezoelectric constant, $\mathbf{e}_{PE}$, of the PE material, and piezomagnetic coefficient, $\mathbf{q}_{PM}$, of the PM material. For ease of comparison, we choose the material properties of BTO and CFO as the reference and define the normalized materials properties of the PE and PM phases as

$$C_{r,Core}\mathbf{I} = \mathbf{C}_{PE}(\mathbf{C}_{BTO})^{-1}, \quad C_{r,Shell}\mathbf{I} = \mathbf{C}_{PM}(\mathbf{C}_{CFO})^{-1}, \quad C_{r,Matrix}\mathbf{I} = \mathbf{C}_{PM}(\mathbf{C}_{CFO})^{-1}$$

and, likewise, are $e_{r,Core}$, $q_{r,Shell}$, $q_{r,Matrix}$, $\kappa_{r,Core}$, $\kappa_{r,Shell}$, $\kappa_{r,Matrix}$, $\mu_{r,Core}$, $\mu_{r,Shell}$, $\mu_{r,Matrix}$. Note that all the components of the material constant are magnified simultaneously for simplicity. Below we numerically compute the ME voltage coefficients $\alpha^*_{E,11}$

Table 1
Material parameters of BaTiO3 (eFunda), $CoFe_2O_4$ (Li and Dunn, 1998b), Terfenol-D (Engdahl, 2000; Nan et al., 2001), $LiNbO_3$ (eFunda), and PZT-5J (eFunda: Nan et al., 2001).

Property	$BaTiO_3$	$CoFe_2O_4$	Terfenol-D	$LiNbO_3$	PZT-5 J
C_{11} (GPa)	150.37	286	8.541	203	82.3
C_{12} (GPa)	65.63	173	0.654	52.9	34.1
C_{13} (GPa)	65.94	170.3	3.91	74.9	30.2
C_{33} (GPa)	145.52	269.5	28.3	243	59.8
C_{44} (GPa)	43.86	45.3	5.55	59.9	21.3
C_{66} (GPa)	43.37	56.5	18.52	74.9	24.1
C_{14} (GPa)	0	0	0	8.99	0
C_{56} (GPa)	0	0	0	8.985	0
κ_{11} (nC^2/Nm^2)	9.87	0.08	0.05	0.39	14.53
κ_{33} (nC^2/Nm^2)	11.08	0.093	0.05	0.26	10.12
μ_{11} ($\mu Ns^2/C^2$)	5	590	8.644	5	1.26
μ_{33} ($\mu Ns^2/C^2$)	10	157	2.268	10	1.26
e_{15} (C/m^2)	11.4	0	0	3.7	14.26
e_{16} (C/m^2)	0	0	0	−2.534	0
e_{21} (C/m^2)	0	0	0	−2.538	0
e_{31} (C/m^2)	−4.32	0	0	0.19	−10.45
e_{33} (C/m^2)	17.36	0	0	1.31	16.58
q_{15} (N/Am)	0	550	155.56	0	0
q_{31} (N/Am)	0	580.3	−5.7471	0	0
q_{33} (N/Am)	0	699.7	270.1	0	0

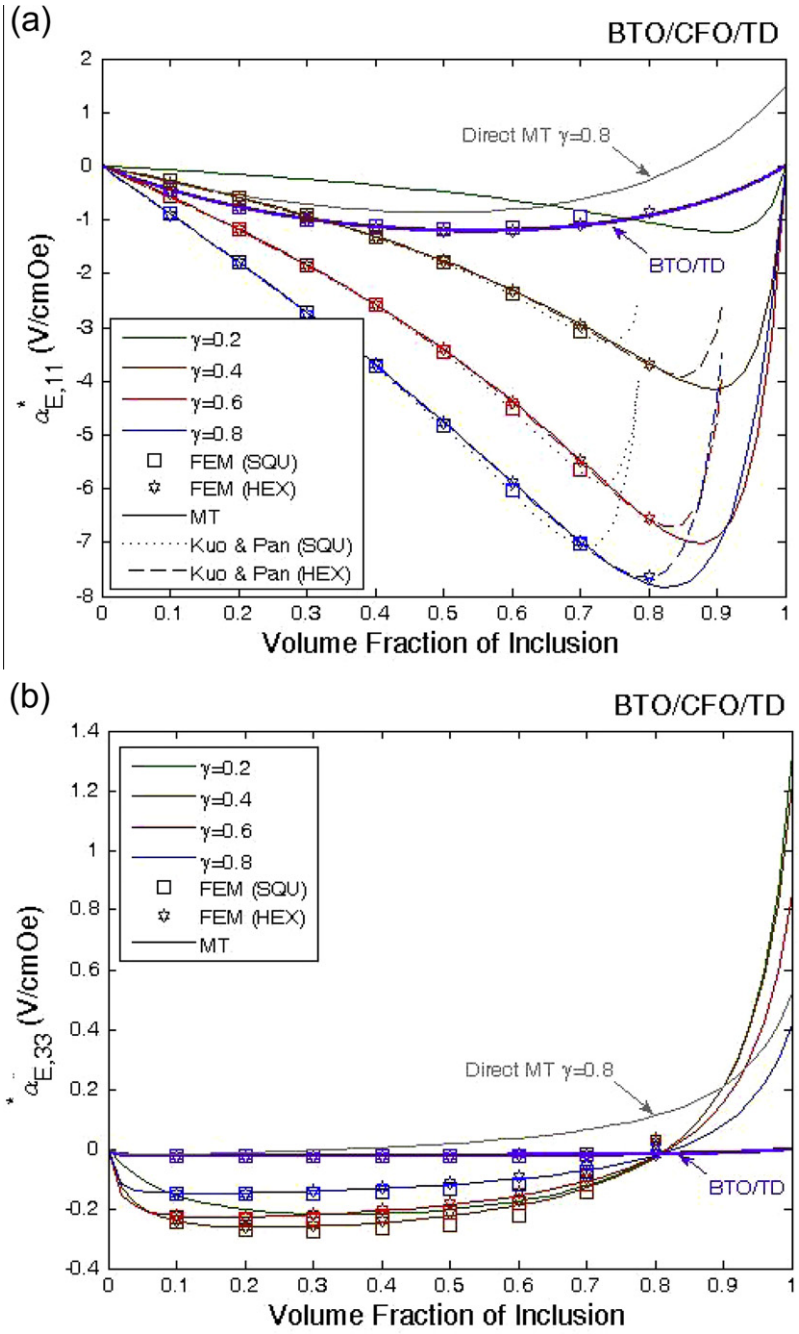

Fig. 3. The predicted ME voltage coefficient vs the volume fraction of inclusion, f_i, and radius ratio, γ, of a BTO/CFO/TD coated fibrous composite: (a) ME voltage coefficient $\alpha^*_{E,11}$ and (b) ME voltage coefficient $\alpha^*_{E,33}$. In both (a) and (b), solid lines are based on the two-level recursive scheme with the Mori–Tanaka model, while discrete point symbols are based on the finite element analysis.

and $\alpha^*_{E,33}$ and their dependence on the normalized material properties of core (PE), shell (PM), and matrix (PM) phases. These results give important guidelines for practical designs of ME coated fibrous composites.

Figs. 4 and 5 show the contours of the normalized effective ME voltage coefficients $\alpha^*_{E,11}/\alpha^0_{E,11}$ and $\alpha^*_{E,33}/\alpha^0_{E,33}$ of a PE/PM/PM composite at the inclusion volume fraction $f_i = 0.5$ and the ratio of the radii $\gamma = 0.8$, where the ME voltage coefficients $\alpha^0_{E,11} = -0.0336$ V/cmOe and $\alpha^0_{E,33} = 0.925$ V/cmOe of BTO/CFO/CFO composite are chosen as the unit for ease of comparison. In Figs. 4(a) and 5(a), the vertical and horizontal axes represent the normalized elastic constants of core and shell phases, respectively, while the variation of matrix's elastic constant is shown by different subplots (a-1,a-2,a-3). The other material

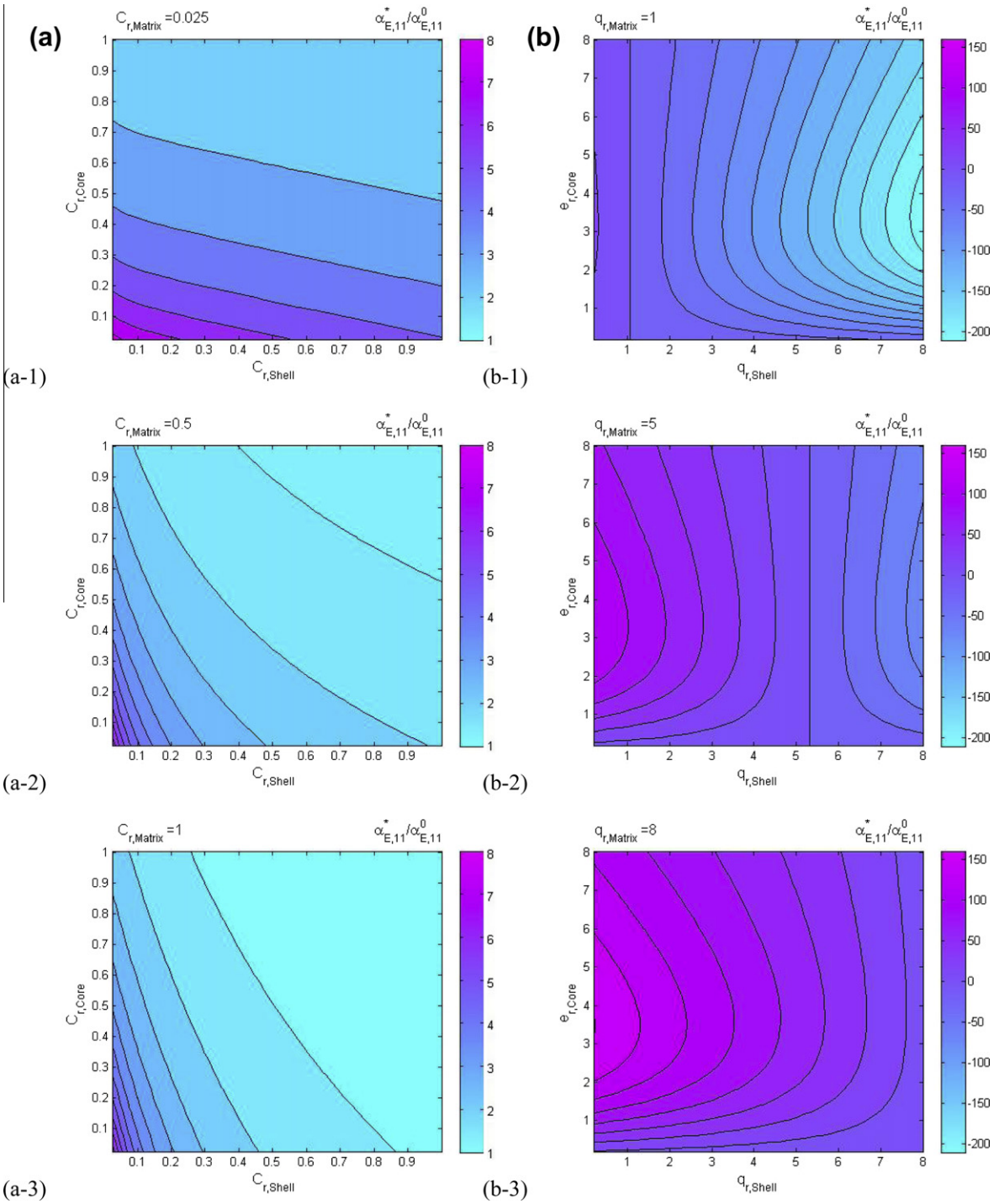

Fig. 4. The predicted in-plane ME voltage coefficient vs different material parameters. The composite is made of PE core phase, PM shell and matrix phases. The volume fraction of inclusion $f_i = 0.5$, and the radius ratio $\gamma = 0.8$. The normalized ME voltage coefficient $\alpha^*_{E,11}/\alpha^0_{E,11}$ vs (a) normalized elastic constants $C_{r,Core}$, $C_{r,Shell}$ and $C_{r,Matrix}$; (b) normalized piezoelectric coefficient of PE core $e_{r,Core}$ and piezomagnetic coefficient of PM shell $q_{r,Shell}$ and matrix $q_{r,Matrix}$; (c) normalized dielectric permittivity $\kappa_{r,Core}$, $\kappa_{r,Shell}$ and $\kappa_{r,Matrix}$; (d) normalized magnetic permeability $\mu_{r,Core}$, $\mu_{r,Shell}$ and $\mu_{r,Matrix}$.

constants are fixed as those of BTO for PE phase or CFO for PM phase. It is observed that the ME voltage coefficient increases when any one of the core, shell or matrix's elastic constant decreases. Therefore, softer PE and PM materials are preferred for improving the ME voltage coefficients of PE/PM/PM three-phase fibrous composites. Figs. 4(b) and 5(b) show the contours of the relative effective ME voltage coefficient versus the piezoelectric and piezomagnetic constants in linear scale. For a fixed

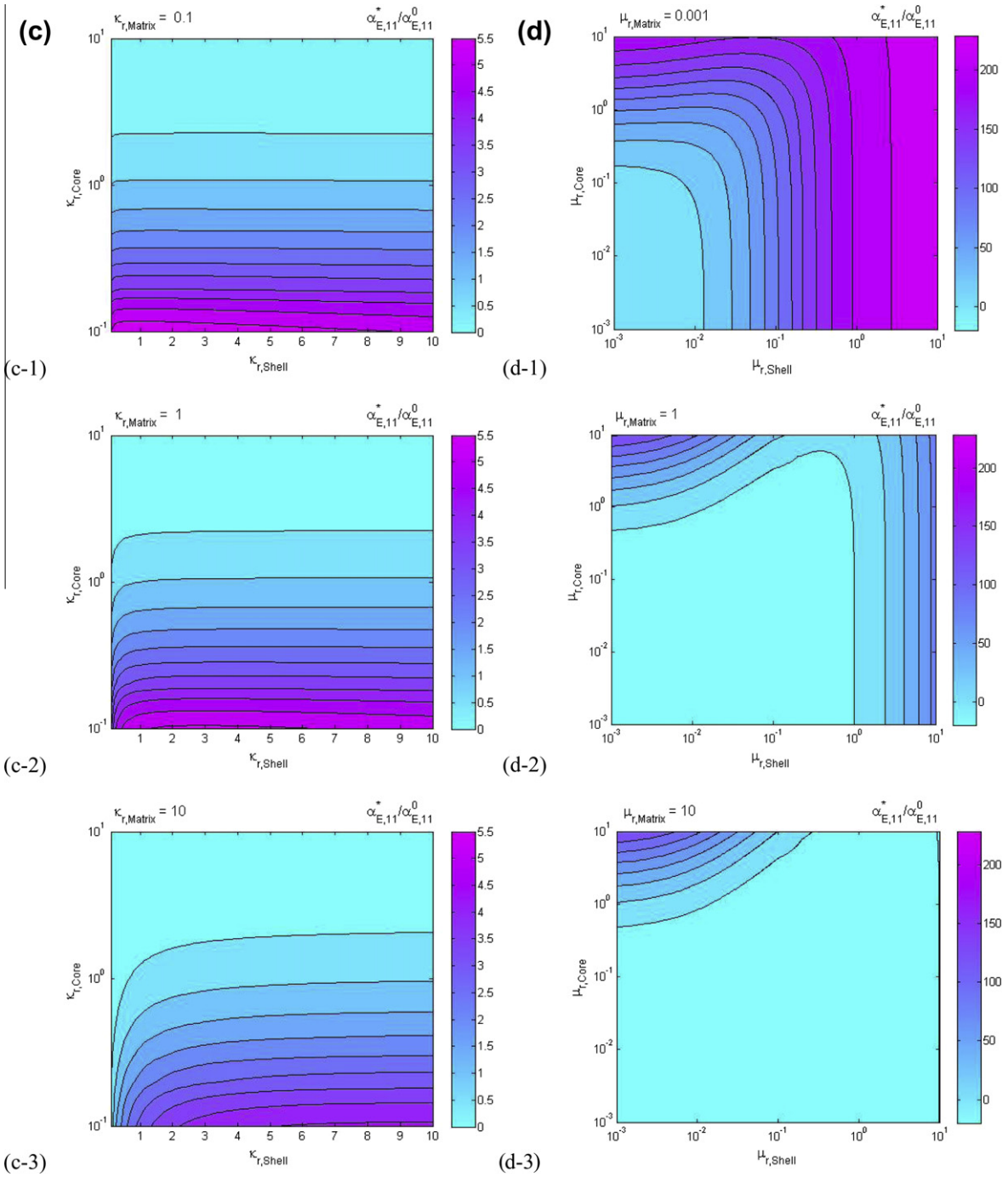

Fig. 4. (*continued*)

normalized piezoelectric coefficient, $e_{r,Core}$, the absolute ME voltage coefficient $\alpha^*_{E,11}$ decreases first and increases after certain minimum as the shell or matrix's piezomagnetic coefficient increases. However, for fixed normalized piezomagnetic coefficients of the shell and matrix phases and as the piezoelectric coefficient increases, the coupling increases first and decreases after certain optimal. Therefore, nontrivial optimal piezoelectric coefficient and lower or higher piezomagnetic constants are preferred for improving the ME effect $\alpha^*_{E,11}$. On the other hand, for the ME voltage coefficient $\alpha^*_{E,33}$, the behavior is quite different (Fig. 5(b)). It is observed that the ME voltage coefficient increases when any of the core's piezoelectric constant, shell or matrix's piezomagnetic constant increases. Therefore, higher piezoelectric coefficient or piezomagnetic coefficient

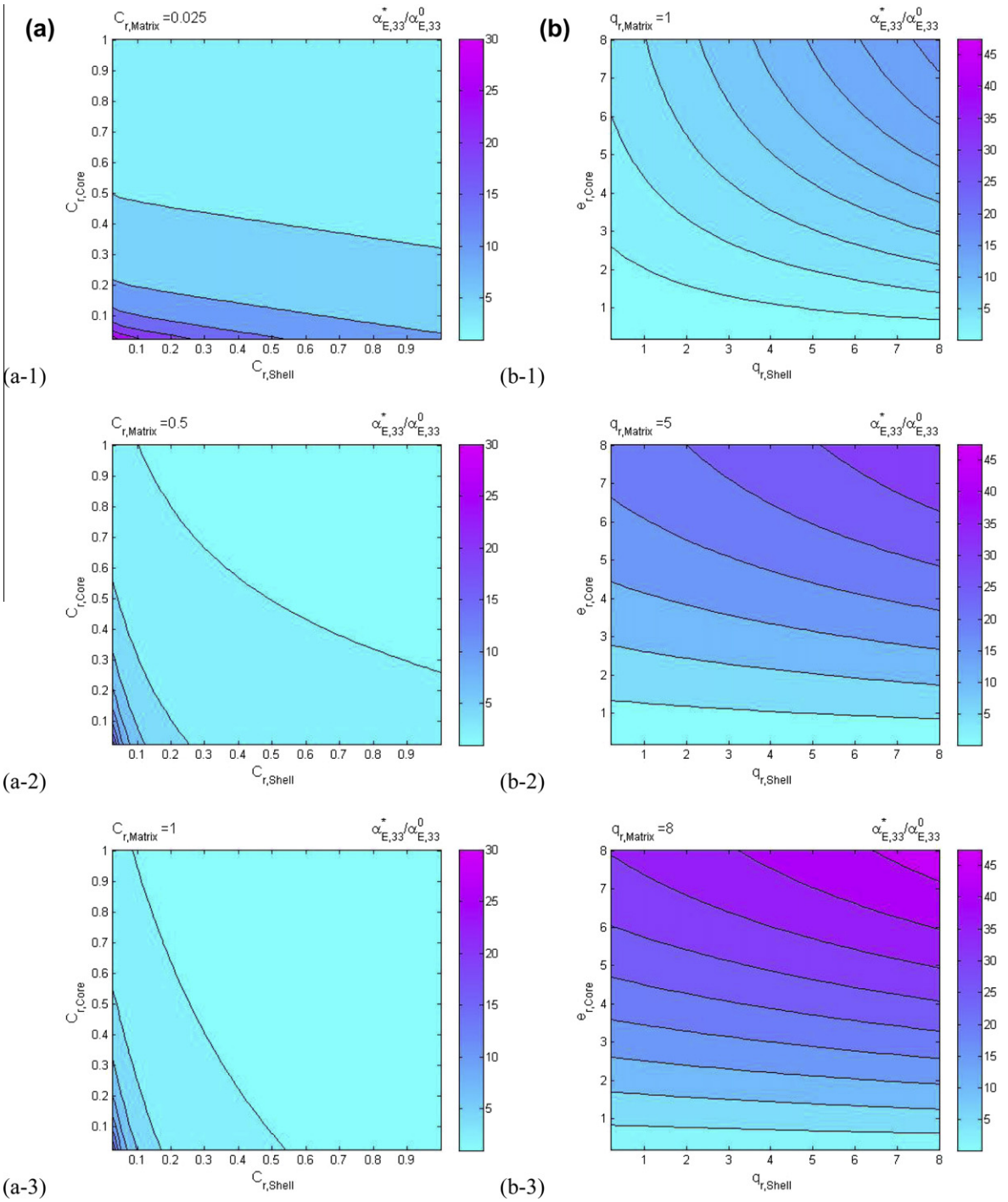

Fig. 5. The predicted out-of-plane ME voltage coefficient vs different material parameters. The composite is made of PE core phase, PM shell phase and PM matrix phase. The volume fraction of inclusion $f_i = 0.5$, and the radius ratio $\gamma = 0.8$. The normalized ME voltage coefficient $\alpha^*_{E,33}/\alpha^0_{E,33}$ vs (a) normalized elastic constants $C_{r,Core}$, $C_{r,Shell}$ and $C_{r,Matrix}$; (b) normalized piezoelectric coefficient of PE core $e_{r,Core}$ and piezomagnetic coefficient of PM shell $q_{r,Shell}$ and matrix $q_{r,Matrix}$; (c) normalized dielectric permittivity $\kappa_{r,Core}$, $\kappa_{r,Shell}$ and $\kappa_{r,Matrix}$; (d) normalized magnetic permeability $\mu_{r,Core}$, $\mu_{r,Shell}$ and $\mu_{r,Matrix}$.

are preferred for improving the ME voltage coefficient in the axial direction. Figs. 4(c) and 5(c) show the contours of the relative ME coupling versus the normalized electric permittivity of PE and PM phases. We observe that the smaller the core's permittivity, the larger the ME voltage coefficients. For the PM shell or matrix's permittivity, however, they only slightly influence the ME effect. Figs. 4(d) and 5(d) show the contours of the relative ME voltage constants versus the normalized

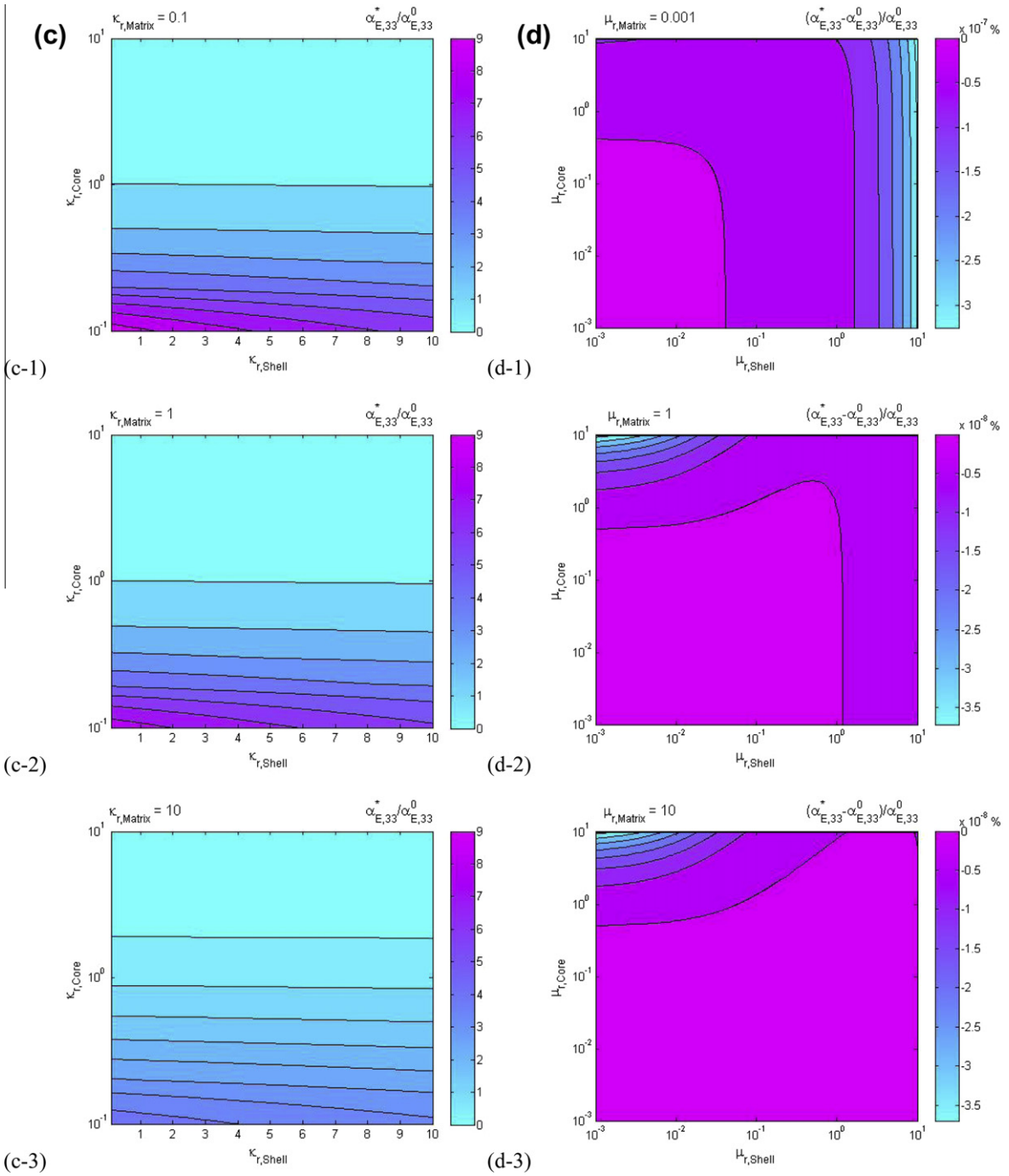

Fig. 5. (*continued*)

magnetic permeability in logarithmic scale. For the in-plane ME voltage coefficient $\alpha^*_{E,11}$, we observe that increasing the PE core's or PM shell's magnetic permeabilities largely enhances the coupling constant, and on the contrary, increasing the PM matrix's magnetic permeability lowers the ME voltage coefficient. Therefore, a large magnetic permeability of the PE core and PM shell and a small magnetic permeability of the PM matrix phase are preferred for improving the in-plane ME voltage coefficient $\alpha^*_{E,11}$. However, the out-of-plane coupling constant $\alpha^*_{E,33}$ is almost independent of magnetic permeability (Fig. 5(d)). For clearness, the contours are shown as the change rate of the ME coefficient, $\left(\alpha^*_{E,33} - \alpha^0_{E,33}\right)/\alpha^0_{E,33}$.

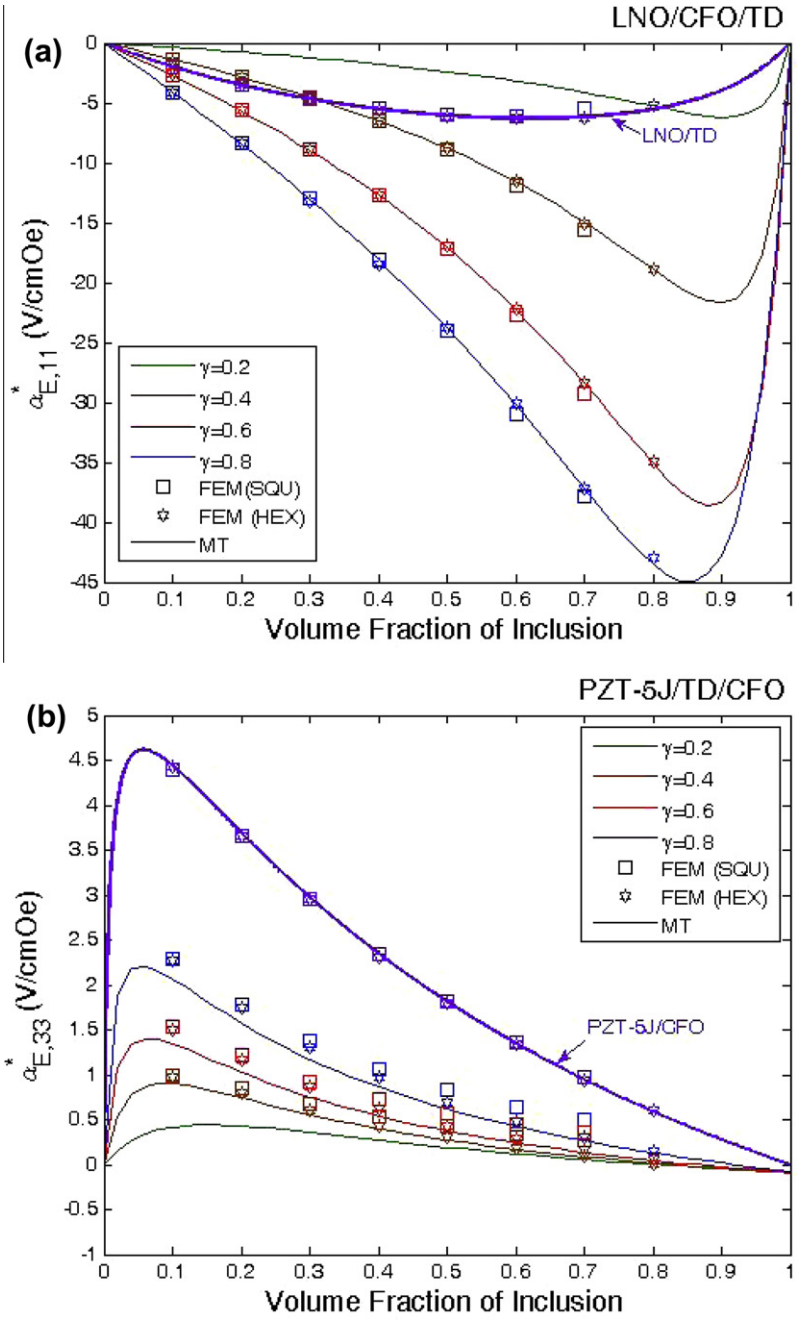

Fig. 6. The predicted ME voltage coefficient vs the volume fraction of the inclusion, f_i, and radius ratio, γ, of a (a) LNO/CFO/TD coated fibrous composite; (b) PZT/TD/CFO coated fibrous composite. In both (a) and (b), lines are based on the two-level recursive scheme with the Mori–Tanaka model, while discrete point symbols are based on the finite element analysis.

Motivated by the above study, we study a ME composite of $LiNbO_3$ (LNO, 3 m symmetry), $CoFe_2O_4$, and Terfenol-D as the core, shell, and matrix phases (Fig. 6(a)), since LNO has lower dielectric permittivity and the matrix TD has lower elastic stiffness and magnetic permeability. The material constants of LNO are listed in Table 1. For this ME composite, the maximum is attained at the volume fraction $f_i = 0.86$ and ratio of the radius $\gamma = 0.8$ where ME voltage coefficient $\alpha^*_{E,11} = -44.9393$ V/cmOe. For the out-of-plane ME voltage coefficient $\alpha^*_{E,33}$, we choose a composite made of PZT/TD/CFO. This is because PZT (6 mm symmetry) has lower elastic constant and higher piezoelectric coefficient, while the shell TD is softer. The maximum occurs at the volume fraction $f_i = 0.06$ and ratio of the radius $\gamma = 1.0$ with coupling constant $\alpha^*_{E,33} = 4.6134$ V/cmOe.

6. Concluding remarks

In this work, a micromechanical approach, the two-level recursive scheme in conjunction with the Mori–Tanaka model, is adopted to estimate the effective moduli of a coated fibrous composites made of PE and PM phases. We have used it to study the dependence of a particular material property of interest, the ME voltage coefficient, on the volume fraction of the inclusion, the ratio of the radii between the core and shell, and the material parameters of the PE and PM phases. The results are compared with the finite element analysis and the semi-analytical method proposed by Kuo and Pan (2011). The magnitudes and trends among them are in good agreement. In addition, for a PE/PM/PM coated fibrous composite with fixed volume fraction and radius ratio, we show that softer materials are desirable for improving the ME coupling. Further, for the in-plane ME voltage coefficient $\alpha^*_{E,11}$, it is desirable to have larger (smaller) magnetic permeability in the PM shell (PM matrix), and smaller dielectric permittivity, but larger magnetic permeability in the PE core. Besides, there exists optimal values of the piezoelectric constant. On the other hand, for the out-of-plane ME voltage coefficient $\alpha^*_{E,33}$, it is desirable to have smaller dielectric permittivity of PE phase, and higher piezoelectric (piezomagnetic) coefficient of the PE (PM) phase. The magnetic permeability has no effect on the ME coupling $\alpha^*_{E,33}$.

In the past decades, some three-phase composites consisting of piezoelectric and magnetostrictive/piezomagnetic phases have been investigated in experiments. However, those composites are either in the form of laminates (Dong et al., 2006) or particulate composites (Gupta and Chatterjee, 2009; Jadhav et al., 2009; Nan et al., 2002, 2003). To the best of authors' knowledge, there is no known experimental result for core–shell-matrix ME fibrous composites. Therefore, we believe that this framework and principles will stimulate new experimental works and shed new light on magnetoelectric coated fibrous composites.

Acknowledgement

We are glad to acknowledge the financial support from the National Science Council, Taiwan, under Contract No. NSC 100–2628-E-009–022-MY2.

References

Aboudi, J. (2001). Micromechanical analysis of fully coupled electro-magneto-thermo-elastic multiphase composites. *Smart Materials and Structures, 10*, 867–877.

Alshits, V. I., Darinskii, A. N., & Lothe, J. (1992). On the existence of surface waves in half-infnite anisotropic elastic media with piezoelectric and piezomagnetic properties. *Wave Motions, 16*, 265–284.

Astrov, D. N. (1960). The magnetoelectric effect in antiferromagnetics. *Soviet Physics JETP, 11*, 708–709.

Bichurin, M. I., Petrov, V. M., & Srinivasan, G. (2003). Theory of low-frequency magnetoelectric coupling in magnetostrictive-piezoelectric bilayers. *Physical Review B, 68*, 054402.

Camacho-Montes, H., Sabina, F. J., Bravo-Castillero, J., Guinovart-Díaz, R., & Rodríguez-Ramos, R. (2009). Magnetoelectric coupling and cross-property connections in a square array of a binary composite. *International Journal of Engineering Science, 47*, 294–312.

Dinzart, D., & Sabar, H. (2011). Magneto-electro-elastic coated inclusion problem and its application to magnetic-piezoelectric composite materials. *International Journal of Solids and Structures, 48*, 2393–2401.

Dong, S., Zhai, J., Li, J., & Viehland, D. (2006). Enhanced magnetoelectric effect in three-phase $MnZnFe_2O_4/Tb_{1-x}Dy_x$ $Fe_{2-y}/Pb(Zr,Ti)O_3$ composites. *Journal of Applied Physics, 100*, 124108.

Eerenstein, W., Mathur, N. D., & Scott, J. F. (2006). Multiferroic and magnetoelectric materials. *Nature, 442*, 759–765.

<http://www.efunda.com/materials/piezo/material_data/matdata_index.cfm>.

Engdahl, G. (2000). *Handbook of giant magnetostrictive materials*. Academic Press.

Fiebig, M. (2005). Revival of the magnetoelectric effect. *Journal of Physics D: Applied Physics, 38*, R123–R152.

Fisher, F. T., & Brinson, L. C. (2001). Viscoelastic interphases in polymer-matrix composites: theoretical models and finite-element analysis. *Composites Science and Technology, 61*, 731–748.

Friebel, C., Doghri, I., & Legat, V. (2006). General mean-field homogenization schemes for viscoelastic composites containing multiple phases of coated inclusions. *International Journal of Solids and Structures, 43*, 2513–2541.

Gupta, A., & Chatterjee, R. (2009). Magnetic, dielectric, magnetoelectric, and microstructural studies demonstrating improved magnetoelectric sensitivity in three-phase $BaTiO_3$-$CoFe_2O_4$-poly(vinylidene-fluoride) composite. *Journal of Applied Physics, 106*, 024110.

Huang, J. H., & Kuo, W.-S. (1997). The analysis of piezoelectric/piezomagnetic composite materials containing ellipsoidal inclusions. *Journal of Applied Physics, 81*, 1378–1386.

Huang, H. T., & Zhou, L. M. (2004). Micromechanics approach to the magnetoelectric properties of laminate and fibrous piezoelectric/magnetostrictive composites. *Journal of Physics D: Applied Physics, 37*, 3361–3366.

Jadhav, P. A., Shelar, M. B., & Chougule, B. K. (2009). Magnetoelectric effect in three phase y $(Ni_{0.5}Cu_{0.2}Zn_{0.3}Fe_2O_4) + (1 - y)$ (50% $BaTiO_3$ + 50% PZT) ME composites. *Journal of Alloys and Compounds, 479*, 385–389.

Kittel, C. (2005). *Introduction to solid state physics*. New Jersey: John Wiley & Sons, p. 8.

Kuo, H.-Y. (2011). Multicoated elliptic fibrous composites of piezoelectric and piezomagnetic phases. *International Journal of Engineering Science, 49*, 561–575.

Kuo, H.-Y., & Wu, T.-S. (2012). Magnetoelectric effect of three-phase core-shell-matrix particulate multiferroic composites. *Journal of Applied Physics*, *111*, 054915.

Kuo, H.-Y., & Pan, E. (2011). Effective magnetoelectric effect in multicoated circular fibrous multiferroic composites. *Journal of Applied Physics, 109*, 104901.

Kuo, H.-Y., Slinger, A., & Bhattacharya, K. (2010). Optimization of magnetoelectricity in piezoelectric-magnetostrictive bilayers. *Smart Materials and Structures, 19*, 125010.

Lee, J., Boyd, J. G., IV, & Lagoudas, D. C. (2005). Effective properties of three-phase electro-magneto-elastic composites. *International Journal of Engineering Science, 43*, 790–825.

Li, J. Y. (2000). Magnetoelectroelastic multi-inclusion and inhomogeneity problems and their applications in composite materials. *International Journal of Engineering Science, 38*, 1993–2001.

Li, J. Y., & Dunn, M. L. (1998a). Micromechanics of magnetoelectroelastic composite materials: average fields and effective behaviour. *Journal of Intelligent Material Systems and Structures, 9*, 404–416.

Li, J. Y., & Dunn, M. L. (1998b). Anisotropic coupled-field inclusion and inhomogeneity problems. *Philosophical Magazine A, 77*, 1341–1350.
Liu, L., & Kuo, H.-Y. (2012). Closed-form solutions to the effective properties of fibrous magnetoelectric composites and their applications. *International Journal of Solids and Structures, 49*, 3055–3062.
Liu, G., Nan, C. W., Cai, N., & Lin, Y. (2004). Calculations of giant magnetoelectric effect in multiferroic composites of rare-earth-iron alloys and PZT by finite element method. *International Journal of Solids and Structures, 41*, 4423–4434.
Liverts, E., Auslender, M., Grosz, A., Zadov, B., Bichurin, M. I., & Paperno, E. (2010). Modeling of the magnetoelectric effect in finite-size three-layer laminates under closed-circuit conditions. *Journal of Applied Physics, 107*, 09D914.
Nan, C. W. (1994). Magnetoelectric effect in composites of piezoelectric and piezomagnetic phases. *Physical Review B, 50*, 6082–6088.
Nan, C. W., Bichurin, M. I., Dong, S., Viehland, D., & Srinivasan, G. (2008). Multiferroic magnetoelectric composites: historical perspective, status, and future directions. *Journal of Applied Physics, 103*, 031101.
Nan, C. W., Cai, N., Liu, L., Zhai, J., Ye, Y., et al (2003). Coupled magnetic-electric properties and critical behavior in multiferroic particulate composites. *Journal of Applied Physics, 94*, 5930–5936.
Nan, C. W., Li, M., & Huang, J. H. (2001). Calculations of giant magnetoelectric effects in ferroic composites of rare-earth-iron alloys and ferroelectric polymers. *Physical Review B, 63*, 144415.
Nan, C. W., Liu, L., Cai, N., Zhai, J., Ye, Y., Lin, Y. H., et al (2002). A three-phase magnetoelectric composite of piezoelectric ceramics, rare-earth iron alloys, and polymer. *Applied Physics Letters, 81*, 3831–3833.
Nye, J. F. (1985). *Physical properties of crystals*. Oxford: Oxford University Press.
Rado, G. T., & Folen, V. J. (1961). Observation of the magnetically induced magnetoelectric effect and evidence for antiferromagnetic domains. *Physical Review Letters, 7*, 310–311.
Spaldin, N. A., & Fiebig, M. (2005). The renaissance of magnetoelecitrc multiferroics. *Science, 309*, 391–392.
Srinivasan, G. (2010). Magnetoelectric composites. *Annual Review of Materials Research, 40*, 153–178.
Srinivas, S., Li, J. Y., Zhou, Y. C., & Soh, A. K. (2006). The effective magnetoelectroelastic moduli of matrix-based multiferroic composites. *Journal of Applied Physics, 99*, 043905.
Srinivas, G., Rasmussen, E. T., Galleogos, J., Srinivasan, R., Bokhan, Y. I., & Laletin, V. M. (2001). Magnetoelectric bilayer and multilayer structures of magnetostrictive and piezoelectric oxides. *Physical Review B, 64*, 214408.
Wu, T.-L., & Huang, J.-H. (2000). Closed-form solutions for the magnetoelectric coupling coefficients in fibrous composites with piezoelectric and piezomagnetic phases. *International Journal of Solids and Structures, 37*, 2981–3009.
Zheng, H., Wang, J., Lofland, S. E., Ma, Z., Mohaddes-Ardabili, L., Zhao, T., et al (2004). Multiferroic $BaTiO_3$-$CoFe_2O_4$ nanostructures. *Science, 303*, 661–663.